Origin of complex fragments from ^{32}S+^{nat}Ag reaction at 37.5 A MeV

D. Benchekroun, B. Cheynis, A. Demeyer, E. Gerlic, D. Guinet, P. Lautesse, L. Lebreton, M T. Magda, M. Stern, A. Chabane, et al.

Institut
de Physique
Nucléaire
de Lyon

Université Claude Bernard

IN2P3 - CNRS

LYCEN 9624
Août 1996

Origin of complex fragments from $^{32}S + ^{nat}Ag$ reaction at 37.5 A. MeV

D. Benchekroun, B. Cheynis, A. Demeyer, E. Gerlic, D. Guinet,

P. Lautesse, L. Lebreton, M.T. Magda*, M. Stern

Institut de Physique Nucléaire de Lyon, IN2P3/CNRS, Université Claude Bernard,

F-69622 Villeurbanne Cedex, France

A. Chabane, P. Désesquelles, A. Giorni, D. Heuer, A. Lleres, J.B. Viano

Institut des Sciences Nucléaires de Grenoble, IN2P3/CNRS, Université Joseph Fourrer,

53 Avenue des Martyrs, F-38026 Grenoble Cedex, France

* *On leave from SUNY Stony Brook, Department of Chemistry, N.Y 11794-3400, U.S.A.*

Origin of complex fragments from ^{32}S + ^{nat}Ag reaction at 37.5 A.MeV.

D. Benchekroun, B. Cheynis, A. Demeyer, E. Gerlic, D. Guinet
P. Lautesse, L. Lebreton, M.T. Magda*, M. Stern
*Institut de Physique Nucléaire de Lyon, IN2P3-CNRS et Université Claude Bernard,
43, Bd du 11 Novembre 1918, F-69622 Villeurbanne Cedex, France*

A. Chabane, P. Désesquelles, A. Giorni, D. Heuer, A. Lleres, J.B. Viano
*Institut des Sciences Nucléaires de Grenoble, IN2P3-CNRS et Université Joseph Fourier,
53, Avenue des Martyrs, F-38026 Grenoble Cedex, France.*

Abstract

Fragment emission from collisions of ^{32}S with ^{nat}Ag at 37.5 A.MeV has been studied with the 4π multidetector AMPHORA. Production of intermediate mass and heavy fragments as well as of light charged particles has been measured. The total charged particle multiplicity and polar angular distributions have been used to select various classes of collisions. Analysis of angular and energy distributions of fragments and light particles in central collisions indicates the formation of a hot source (excitation energy of ≈ 4.4 A.MeV) with an additional contribution from a preequilibrium process at more forward angles. Azimuthal angle correlations of He - Li, Li - Li, B - B, and C - C pairs have been used as a tool to study the origin of complex fragments. Data at backward angles are well described by considering a thermalized emitter with an angular momentum around 70 $\hbar$ and a fragment emission time of the order of 200 fm/c. A microscopic approach of BNV type confirms these emission times and angular momenta indicating the persistence of an incomplete fusion process responsible for the emission of complex fragments at backward angles.

PACS number(s) : 25.70 Pq

---

* On leave from SUNY Stony Brook, Department of Chemistry, N.Y 11794-3400, U.S.A.

1. INTRODUCTION

The high excitation energies involved in heavy ion collisions at intermediate energies give rise to new decay modes, while those observed at lower incident energies fade out. The emission of complex fragments, alternatively called intermediate mass fragments (IMF), represents a major mode of disassembly of the hot nuclei formed in these reactions [1]. In this paper we use the term "complex fragment" as defined in [2], i.e. reaction products of charge $3 \leq Z \leq 20$. While fragment emission occurs at lower incident energies with quite small cross sections [2-4], it becomes an important decay mode of highly excited nuclei [2, 5-9]. The emission of many fragments or *multi-fragment* emission in the decay of massive nuclei has been observed for excitation energies of ≈ 3 A·MeV. There is a transition from sequential emission to multifragmentation [10] when going up in excitation energy (≈ 5 A·MeV).

Much theoretical and experimental work has been dedicated to finding a criterion for a clear distinction between prompt *multifragmentation* and sequential *multi-fragment* emission, either by looking for kinematic differences in the Coulomb trajectories of fragments [11, 12] or by using nuclear interferometry methods [6, 13, 14]. The sensitivity of the relative velocity between fragments to the decay mechanism offers another tool that has been used to explore details of the emission process [9, 15, 16]. The problem is not a trivial one and needs further investigation. Difficulties are due to intrinsic properties of the explored phenomenon, namely the decrease of fragment emission time with increasing excitation energy to such extent that a distinction between "prompt" and "short delayed sequential" no longer exists. In this context we have resumed an earlier study of the ^{32}S + ^{nat}Ag system at 30 A·MeV [17, 18]. In this study complex fragments were observed to originate from a compound nucleus - like source formed in an incomplete fusion reaction with a linear momentum transfer of 80%. This paper deals with emission dynamics and presents new results obtained at a higher incident energy of 37.5 A·MeV [19, 20] where more abundant fragment production is expected.

In section 2 the experimental setup is described followed in section 3 by a presentation of the method adopted to select peripheral and central event classes, with a particular emphasis on azimuthal angle correlations. Section 4 contains a detailed presentation of

2

the analysis of azimuthal angle correlations, namely the method to define the emitter of complex fragments. Emission times and angular momenta of the rotating source extracted from the analysis of He - Li, Li - Li, B - B, and C - C azimuthal angle correlations are presented and discussed in the context of a microscopic approach.

2. EXPERIMENT

2.1 Accelerator and detection method

Experimental data were obtained with a 37.5 A·MeV ^{32}S beam on a target of 500 μg/cm^2 natural Ag [20]. Measurements were made with the 4π multidetector AMPHORA [21,22] at the SARA facility. The AMPHORA detector has a geometrical efficiency of 82.7% of 4π which enables a sufficient phase - space coverage to acquire nearly complete information on complex fragments together with other reaction products : light charged particles (Z=1 and 2) and heavy residues. A detailed description of the AMPHORA multidetector has been given elsewhere [21, 22]. Here we shall only point out the specific details relevant to the present experiment [20]. Light charged particle isotopes were identified in all CsI modules of AMPHORA with a detection threshold of $\approx$ 2 A·MeV. Li and heavier fragments (Z$\geq$4) were identified by charge. Plastic detectors (NE102) were coupled to CsI detectors in a phoswich ensemble, starting from 4° up to 31°, allowing identification of fragments of charge less than 20, with an energy threshold of 5-6 A·MeV. In order to achieve a better identification five plastic detectors have been replaced by Si(Li) detectors of 300 μm thickness, three of them placed at a polar angle of 8°, the other two at 12° and 14°, respectively. In order to detect slow fragments ionization chambers with a lower detection threshold replaced three plastic detectors in the wall of AMPHORA at polar angles of 8°, 12°, and 14°. For the detection of heavy residues the measurement of energy and time - of - flight allowed to determine their masses.

2.2 Data acquisition and processing

The energy calibration of the detectors has been performed carefully in a separate measurement with the same beam and target as above. Inclusive energy and angular distributions were measured with Si - telescopes and channel plate time - of - flight detectors, using a reaction chamber equipped with movable detector holders. The energy spectra

3

acquired this way were taken as a reference for the energy calibration of the AMPHORA detectors. The configuration of the telescope for light charged particle and fragment calibration included three Si detectors of 40, 150, and 500 μm thicknesses followed by a 3 cm thick CsI(Tl) scintillator. The Si detectors were calibrated with α particles from a ^{242}Cm source together with the punch-through energies of various particles. The non-linear response of CsI, especially in the case of Z$\geq$3 particles has been taken into account using the existing recipes [23]. A second group of detectors included two Si-detectors of 150 and 2000 μm, and two channel plate time - of - flight detectors for the calibration of energy and time - of - flight spectra of heavy residues. The reference quantities were given by the elastic scattering of ^{32}S at 37.5 A·MeV on a Au target. The flight path of 64 cm was long enough for the separation of the heavy residues.

The elaborate data processing has been performed using the DALI software package [24]. In the case of plastic detectors, the most difficult identification of elements of $Z > 2$ has been done with a program [25] which fits the data with contours corresponding to successive elements. The uncertainty on charge identification is one unit for elements up to Z=10, and 2 units for $Z > 10$ elements.

3. SELECTION OF REACTION CLASSES

An important production of IMF has been observed. Fig. 1 shows the probability distribution of IMF emitted in the whole AMPHORA with no trigger imposed (black stars). Since the data have not been corrected for the filter effect of the multidetector these fragment numbers should be considered as lower limits. We see in Fig. 1 that up to three IMF per event are produced with noticeable probability. The IMF yield decreases dramatically, roughly exponentially in the case of large numbers of IMF. The difficult problem one faces concerns the origin of these IMF ; by identifying the source one can obtain information about its characteristics. With this goal in mind we have explored various observables that allow to select particular classes of events.

Light charged particle (LCP) multiplicities have frequently been used to distinguish central from peripheral collisions [2, 26, 27]. Total charged particle multiplicity has also been adopted in the present work for selecting various reaction classes according to the

4

associated centrality.

The total charged particle multiplicity M is determined for each event by the number of detectors in which at least one charged particle is detected, including light particles and complex fragments. A collision impact parameter has been determined based on geometrical arguments for the quantity M. The method has been presented in details in [28, 29]. We only recall that it relies on the assumption that there is a monotonic relation between the impact parameter and charged particle multiplicity, so that to a variation of the impact parameter db one can associate a variation $dP(M)$ of total particle multiplicity

$$\frac{2\pi \ bdb}{\pi b_{max}^2} = -dP(M) \tag{1}$$

where b_{max} is the maximum impact parameter and $dP(M)$ represents the probability for the multiplicity to be found in the interval M, $M + dM$. The negative sign indicates that the largest multiplicities, i.e. M values, are associated to more violent collisions, namely to small impact parameter values b. By integrating eq. (1) a relation can be deduced between the reduced impact parameter ($\frac{b}{b_{max}}$) and charged particle multiplicity:

$$\left(\frac{b}{b_{max}}\right)^2 = \int_M^\infty \frac{dP(M)}{dM} dM \tag{2}$$

Here $dP(M)/dM$ denotes the normalized probability of charged particle multiplicity. Its distribution (uncorrected for detector acceptance) is given in Fig. 2a. The correlation between the reduced impact parameter and multiplicity is shown in Fig. 2b. The maximum value of the impact parameter has been deduced from the reaction cross section σ_R, with the well known relation : $\sigma_R = \pi b_{max}^2$. A semi-empirical model adequate for heavy ion reactions at intermediate energies has been used for estimating the reaction cross section [30, 31]. Thus a value of 3.7 b has been obtained for σ_R, which leads to $b_{max}=10.8$ fm.

It is important to check if the assumed relationship between impact parameter and particle multiplicity is not destroyed by the acceptance of the multidetector AMPHORA. This effect has been investigated by simulating the total multiplicity - impact parameter correlation *without* and *with* the AMPHORA filter. In the simulation the model [32] calculates the trajectories of the colliding nuclei by solving the classical dynamical equations. Nuclear and Coulomb forces were included in the calculations as well as dissipative ones

(nuclear friction). Depending on the impact parameter, the collision leads either to fusion of the two collision partners or to an elastic/inelastic process with the formation of target-like and projectile - like nuclei. Preequilibrium emission is taken into account using the model of Blann [33]. The resulting nuclei are assumed to deexcite by successive binary splittings [34]. The simulations demonstrate that the particle multiplicity - impact parameter correlation still holds when the filtering effect of the detector acceptance is taken into account. This result supports the use of the total multiplicity for determination of the impact parameter and therefore the reaction class. However due to increasing fluctuations of the charged particle multiplicity related to lower values of the impact parameter, we adopted "slices" of multiplicity for selecting various reaction classes. The chosen multiplicity intervals (denoted ΔM) were the following : ΔM_1=1-7 (peripheral collisions), ΔM_2=8-13 (semi-central collisions) and ΔM_3=14-22 (central collisions). The impact parameter values associated to these multiplicity intervals are indicated by arrows in Fig. 2b.

The effect of these multiplicity gates on the IMF multiplicity distribution is shown in Fig. 1. The measured distributions relative to the "not gated" one are shown, not filtered by the response of the experimental apparatus. The shift of the multiplicity distribution toward higher values of multiplicity when going from peripheral to central collisions is observed. We notice that the maximum of the distribution for peripheral collisions, corresponding to ΔM_1, is located at $M_{IMF} = 0$ with an abrupt decrease at larger multiplicities. In both semi-central (ΔM_2) and central collisions (ΔM_3) the maximum of the distribution is at $M_{IMF} = 1$ with a significant amount of 2 to 3 IMF events when compared to ΔM_1. This result supports the conclusion that multiple fragment emission is related to more central collisions.

Other selection criteria have been explored, as for example, the number of IMF detected in the event (M_{IMF}) and its dependence on polar angle. The effect of gating on IMF number has been investigated in detail in reference [20]. An interesting result is the dependence of the average total charged particle multiplicity $\langle M \rangle$ on the emission angle of one (at least) detected IMF (Fig. 3). After a sharp increase of the average multiplicity associated with an IMF in the angular range $\theta = 4° - 14°$, the average multiplicities reach

an approximately constant large value. This result indicates that IMF's emitted at θ larger than 16° are associated to collisions with highest energy deposition, thus suggesting that azimuthal correlations between two fragments detected at angles $> 16°$ may be used to study the characteristics of a highly excited emitter. This effect is better illustrated in Fig. 4 which shows the total multiplicity triggered by fragments detected at angles larger than 16°. Total charged particle multiplicity distributions obtained from events in which at least one IMF has been detected anywhere in the AMPHORA detector (black circles) and those gated by either at least one (open circles) or two Li fragments (triangles) detected in the 16° - 78° angular range are presented in Fig. 4. The three multiplicity intervals chosen for gating on various classes of reactions indicated by vertical lines, emphasize the fact that the Li fragments are mostly related to semi-central collisions. We deduced an average charged particle multiplicity of 10.2, which is higher than 8.2 obtained for the $^{32}S +^{nat}Ag$ system at 30 A·MeV [17]. Such an increase of the total multiplicity indicates that the reaction class characterized by the emission of at least two fragments at polar angles larger than 16° is associated with high energy deposition which still increases when going up in incident energy from 30 to 37.5 A·MeV.

Based on the results presented here, total particle multiplicities and polar emission angles have been used in this work to separate central and semi-central from peripheral collisions.

4. ANALYSIS OF AZIMUTHAL ANGLE CORRELATIONS

Fragment - fragment correlation measurements provide a useful piece of information for investigating the dynamics of fragment emission. In the region of incident energies of a few tens of A·MeV, azimuthal distributions reflect the influence of a rotation - like behaviour of the emitter in addition to sidewards flow [13, 35-41]. Previous measurements of azimuthal angle correlations between light particles and/or fragments with the multidetector AMPHORA [38, 41] have demonstrated its suitability for this type of experiment. In the present work, azimuthal correlations have been measured for fragments emitted into the "ball"region of the multidetector array, i.e. in the range of polar angles of $\theta =$ 16° - 78°. The detectors located in this part of the "ball" have a geometry well suited to

7

angular correlation measurements, being disposed in four rings centered at polar angles of $20°, 31°, 47°$, and $67°$ each containing the same number of detectors (15) with a cylindrical symmetry with respect to the beam axis.

The azimuthal correlation function is defined [42] as :

$$C(\Delta\varphi) = Y(\Delta\varphi)/Y'(\Delta\varphi) = A[1 + R(\Delta\varphi)] \tag{3}$$

where $\Delta\varphi$ is the difference between the azimuthal angles φ_1, φ_2 of the two charged products. Y represents the distribution of correlated pairs while Y' is the distribution of mixed event uncorrelated pairs. The normalization constant A is determined in such a way that the average value of $(1 + R(\Delta\varphi))$ is equal to unity.

In our experiment, the detectors within a ring have comparable efficiencies so that the relative intensity of uncorrelated pairs with the same polar angles (θ_1, θ_2) and $\Delta\varphi$ is practically the same. This point has been checked with the AMPHORA detector [41] where it was shown that $\Delta\varphi$ distributions constructed for mixed events are flat.

4.1. Empirical parameterization of the correlation function

In a first approach the experimental correlations $C(\Delta\varphi)$ have been fitted as in reference [43] using the following expression :

$$C(\Delta\varphi) = 1 + \lambda_1 cos(\Delta\varphi) + \lambda_2 cos(2\Delta\varphi) \tag{4}$$

The parameters λ_1 and λ_2 give information on the emission process, namely rotation - like behaviour of the emitter, recoil effects, final state interaction and flow phenomena [44,45]. Large λ_2 values can be related to collective motion of the nucleus, such as rotation. Positive values of λ_1 indicate a preferential emission of the particle pair at $\Delta\varphi = 0°$ and reflect final state interaction effects such as the decay of particle unstable fragments. Negative values of λ_1 reflect an anisotropy $0° - 180°$ due to Coulomb repulsion between the two particles or to momentum conservation. In this work azimuthal angle correlations between identical pairs of light particles and Li fragments in the polar angular range $16°$-$78°$ have been studied. We have used the parameters λ_1 and λ_2 to study the evolution of these angular correlations with the reaction class and therefore with the impact parameter. λ_1

8

and λ_2 values obtained by fitting the experimental correlations of various pairs are shown in Fig. 5 versus the reduced impact parameter b/b_{max}. Both ^{3}He and ^{4}He have been included in these He - He pairs. The azimuthal correlations were determined for various multiplicity gates which may be associated with the impact parameter, as shown in section 3. One can see that for all pairs considered, λ_2 increases as the impact parameter increases. The small, nearly zero, values of λ_2 in the region of small impact parameters confirm the correct selection of central collisions using the particle multiplicity criterion. On the other hand, for a given value of the impact parameter there is a continuous increase of λ_2 when going from ^{1}H - ^{1}H to heavier He - He and Li - Li pairs. This emphasizes the fact that collective effects are stronger and thus more easily observed with heavier pairs [45]. The large λ_2 values for peripheral collisions may be associated with the occurence of a binary process in which target and projectile contribute to the large anisotropy.

The dependence of the parameter λ_1 on the impact parameter is strongly correlated with the particle pair since it reflects distortions due to final state interactions and momentum conservation effects. A change of sign is observed in the case of He and ^{3}H pairs when going from peripheral to central collisions. In case of He pairs, the small positive values of λ_1 observed for small impact parameters are presumably due to ^{4}He pairs coming from ^{8}Be decay. The λ_1 values extracted from Li - Li correlations are always negative and have absolute values greater than those obtained for ^{1}H, ^{2}H, and ^{3}H pairs. This is understandable as the Coulomb repulsion is more important in the case of higher Z pairs such as Li.

Such an analysis has been extended to pairs of non - identical products, as for example He - Li and d - He. Here also we have found positive values of λ_1 for low impact parameter. Moreover the values of λ_2 are intermediate between those obtained for the relevant identical pairs. He - Li pairs will be analyzed in further detail later. Finally, the result of the phenomenological parameterization of the azimuthal angle correlations supports the reaction class selection criterion.

4.2. Statistical model

The measured angular correlations were analyzed considering the emission of complex

particles from a hot and rotating emitter at thermal equilibrium. If one treats the emission process within a classical statistical model [46, 47] the probability $W(\phi)$ for a particle to be emitted at an angle ϕ with respect to the direction of the emitter angular momentum is given by the following relation :

$$W(\phi) \approx exp[-\beta cos^2(\phi)] \qquad (5)$$

The anisotropy parameter β is the ratio of the classical centrifugal energy of the emitted particle at the barrier radius over the temperature of the emitter. Therefore it depends on the reduced mass and the radius of the emitted particle and the temperature of the emitter. The salient feature of eq. (5) is the preferential in - plane emission of particles/fragments, as observed in the experimental data, when J increases.

The MODGAN code [48] which is based on the statistical model of nuclear reactions has been used for comparison with measurements. This code follows the deexcitation of a spherical nucleus by light particle as well as complex fragment evaporation. We do not dwell on the statistical model ingredients of the MODGAN code, but only point out some features of the code that make it suitable for treating angular correlation data obtained with a multidetector array like AMPHORA. The actual geometry of the experiment (polar and azimuthal angles of each detector) is taken into account in the input data so that the angular correlations of interest can be computed. The detection thresholds are also given in the input data flow of the code. Moreover, their effects on the results of simulations have been examined by performing simulations with and without the detection threshold used in the experiment. The results obtained in the two cases are quite close for the lighter IMF. The time distribution of emitted particles is assumed to be of the form : $P(t) \approx e^{-\frac{t}{\tau}}$ where τ is a characteristic timescale for the emitter representating the time interval between two successive particle emissions. If required the interaction between two particles is taken into account by calculating their trajectories in the Coulomb field. The key parameters are those related to the characteristics of the emitter, namely the lifetime of the emitter and the angular momentum. Another delicate problem when performing such simulation is the choice of the emitting nucleus due to the increasing contribution of preequilibrium emission at higher energies [49, 50].

4.3 Signature of the emitter

As inputs to the MODGAN code, the velocity, mass and charge as well as the excitation energy of the emitting nucleus have to be selected. An effective emitter velocity was determined using the heavy residue measurements by the time - of - flight method described in section 2.2. The angular distribution of evaporation residues resulting from the simulations has been checked to have a maximum at $\theta_{lab}=8°$ and the mean velocity of evaporation residues remains independent of the angle. The histogram in Fig. 6 shows the velocity spectrum of heavy fragments detected at $\theta_{lab}=8°$. Despite the experimental detection threshold of 0.6 cm/ns, one can clearly see a broad distribution of "evaporation residue - like" fragments. The "shoulder" at low velocity indicates products from a deep inelastic process. In the spectrum gated by high total multiplicity gate (ΔM_2 and ΔM_3) the distribution becomes narrower and remains centered on a velocity of 1.4 cm/ns. Target-like products are eliminated. This experimental value of 1.4 cm/ns represents 72% of the center - of - mass velocity indicating an incomplete fusion process involving a substantial contribution of preequilibrium emission at energies above 30 A·MeV [17, 49, 50].

The multiplicity and energy distribution of light particles and Li fragments as a function of polar angle can help to determine the other characteristics of the emitting source. The energy distributions of Li fragments emitted between 16° and 78° have been analyzed using a source moving with 1.4 cm/ns velocity [20]. At backward angles a good fit is obtained with a temperature T of the emitter of $\approx$ 6.5 MeV. This value is in agreement with the temperature of $\approx$ 7 MeV found from an analysis performed over the same angular emission range for α particles. With such temperatures and a level density parameter of A/10 a mean excitation energy per nucleon of $\epsilon \approx$ 4.4 A.MeV is determined. However such a relaxed source is not sufficient to describe energy spectra of light particles and Li at forward angles : an additional emission source, with a velocity of one third of the projectile velocity and a slope parameter of 9 MeV, is required. This analysis indicates that the major contribution comes from the preequilibrium stage at forward angles and from the equilibrated system at angles larger than 31°. We note that additional yield is observed in singles distributions at angles smaller than 16° and is associated with a source whose velocity is close to the projectile one. However in events triggered by high total

11

multiplicity (ΔM_3) such a contribution is negligible.

The effective mass of the emitter has been checked using the kinematical model developped by Cerruti et al. [51]. It simulates the reaction mechanism in a two stage model. Preequilibrium emission of particles from the composite system is responsible for the loss of linear momentum. Using the nucleon-nucleon interaction picture which assumes a half projectile mean velocity for this process, 28 preequilibrium nucleons are necesssary to reproduce the observed mean residue velocity of 1.4 cm/ns. The effective composite mass deduced this way is 112 with a total excitation energy of around 500 MeV. With such a thermalized emitter, a total amount of 34 amu of evaporated particles has been extracted for the equilibrated stage. So the final mean residue mass is close to 78±2 amu which is in agreement with observed time-of-flight measurement (Fig.6).

Deduced emitter characteristics are A_0=112, Z_0=48, v_0=1.4 cm/ns with a total excitation energy of 500 MeV. Variations of 10 to 20% to each parameter of the emitter do not change the further conclusions.

4.4 Extraction of angular momenta

The experimental angular correlations between not gated He and Li observed in different rings are displayed in Fig. 7. We observe an evolution from asymmetrical distributions at small polar angles (20° and 31°) to more symmetrical distributions at larger polar angles. The observed extra yield at small $\Delta \varphi$ could be associated with a "preequilibrium component" not included in the model; so the calculations could not fit the data and prevent testing the sensitivity of the emission time to polar angle. The angular momentum has been extracted as a function of polar angle. For angles 47° and 67° a mean J value of 70 ±5$\hbar$ is required. At more forward angles the angular momentum increases up to 80 - 100 $\hbar$. Experimentally the same correlation is obtained for a given angle pair when the two particles are interchanged as for example with He (20°) - Li (31°) and He (31°) - Li (20°). We recall (see section 4.3) that the He energy and angular distributions have indicated a thermalized component at larger angles with a preequilibrium component superimposed at forward angles. The similar behavior of He and Li could lead to assume a non equilibrium component at angles 20° and 31° for Li fragments and a thermalized one at larger angles.

12

Therefore the mean J value of 70 $\hbar$ at backward angles should be seen as characteristic of the thermalized emitter. The higher value of around 100 $\hbar$ at more forward angles must be considered (similar to the slope parameter) only as a parameter used to simulate the azimuthal distributions of a preequilibrium source. In addition it was checked that the angular correlations at backward angles do not change when selecting multiplicity bins.

The analysis has been extended to heavier fragment pairs where one expects stronger recoil and Coulomb effects in the final state and therefore a larger $0°$ - $180°$ anisotropy. Angular momenta of 65 $\hbar$ are needed to reproduce the Li - Li correlations at backward angles [20]. Unfortunately heavier fragments could not be identified at angles larger than $31°$. Fig. 8 presents the angular correlations for Li - Li, B - B and C - C observed at angles $20°$ and $31°$. The angular momenta extracted for heavier fragments for a given configuration of angles are similar to those - here 100 $\hbar$ - deduced from the lighter fragments with the same signification as above.

4.5 Extraction of timescales

The Coulomb interaction between two particles affects the correlation only at small $\Delta\varphi$, the rest of the correlation being unchanged. Moreover since it is a small effect, good statistics are required. Therefore the azimuthal correlations at $20° - 31°$ where the cross sections are largest were analyzed (see Fig. 8). The shorter the time interval τ between emissions, the stronger is the Coulomb repulsion between fragments which induces a depletion of particles at small relative azimuthal angles. The sensitivity of the effect to the emission time of a given emitter (v_0, E_0, A_0, J_0) has been investigated. The best fit to the experimental data as shown in Fig. 8 gives an average time between the emission of the two carbon and boron fragments of 2 and 5 10^{-22}s or (60 and 150 fm/c) respectively. In the case of lithium fragments we estimate the emission time at about 20 10^{-22}s.

We have pursued the analysis of the Li($31°$)-Li($47°$) data (see Fig. 9) for which we also have good statistics. In this case the best fit is obtained with a value of approximately 7 10^{-22}s or 200 fm/c. The analysis has been extended to He - Li correlations at different polar angles. To fit azimuthal correlations at backward polar angles while limiting the contribution of non equilibrium processes, emission time values as high as 50 10^{-22}s or

600 fm/c are necessary, as displayed in Fig. 7. The same time value has been carried throughout the simulations for all polar angle contributions contained in the matrix of He - Li correlations, including forward angles. In the latter case, simulations based on statistical model cannot reproduce all the measured yield, so that the involved time should be understood as characteristic of the part related to emission from an equilibrated emitter. At this point, it is observed that bigger are the fragments, lower are the time intervals. Such a behavior of emission times is in agreement with predictions for light particle and fragment emission from a highly excited equilibrated emitter. Indeed we have explored the structure of the decay cascade calculated by MODGAN for the emitter used in azimuthal correlation simulations and determined the average emission times of various products, using the branching ratios at each step of the decay chain as a weighting factor. An average emission time of $\approx 300 \ 10^{-22}$s was obtained for α particles, and $\approx 2 \ 10^{-22}$s, 10^{-22}s, $0.75 \ 10^{-22}$s for Li, B, and C respectively. Therefore model simulations confirm the evolution of emission times when going from light particles to heavy fragments. On the other hand the small time values resulting from both experiment and simulations in case of heavy fragments stress the point mentioned above. When the excitation energy of the emitter is large, the expected emission time decreases to low values and it is difficult to distinguish between "prompt" and "short delayed" sequential emission.

4.6 Discussion

Emission timescales extracted from measurements of the ^{32}S + ^{nat}Ag system at 37.5 A·MeV incident energy are in good agreement with those found in the literature. Li-Li azimuthal correlations for the ^{40}Ar + ^{nat}Ag system at 27 A·MeV incident energy [41, 48] yielded a delay time between emission of the two Li fragments of 150 fm/c. A decrease of fragment emission time from 500 fm/c to 50 fm/c has been observed for the ^{40}Ar + Au system in going from 30 to 60 A·MeV [14] incident energy corresponding to an increase in the excitation energy of the emitter of 3 to 5 A·MeV. A similar behavior has been determined from momentum correlation functions for Kr + Nb, namely a change from $\tau \approx 400$ fm/c at 35 A·MeV to a value of $\tau \approx 125$ fm/c at 55 A·MeV and above up to 75 A·MeV beam energy [52]. Systematic emission timescale measurements for the

14

$^{40}Ar + {}^{nat}Ag$ reaction at lower beam energies also indicate a decrease from 500 fm/c at 17 A·MeV to 60 fm/c at 34 A·MeV [53]. These time values strongly depend on the particles or fragments in the selected pair and also on the trigger conditions. For example, even at incident energies as high as 34 A·MeV time delays of 600 fm/c are obtained for deuteron-deuteron correlations when selecting only the lowest part of the energy spectrum.

The fragment emission results for the $^{32}S + Ag$ reaction at 37.5 A· MeV obtained within the phenomenological treatment of a hot and fast rotating nucleus are supported by microscopic Boltzmann-Nordheim-Vlasov (BNV) calculations [54]. We have used BNV simulations in order to study the first stage of the reaction, particularly to determine the relationship between impact parameter and reaction type. The calculated transferred angular momenta J are displayed in Fig. 10. Fusion no longer occurs for an impact parameter beyond b $\approx$ 5 fm, being replaced by deep inelastic processes. Then a di-nuclear system is formed in which the two centers of mass (quasi-projectile and quasi-target) can be distinguished. The evolution of this system is accompanied by preequilibrium emission which ceases at t = 120 fm/c. The two fragments separate at t = 200 fm/c involving a maximum J value of 30 $\hbar$. This time decreases for larger impact parameters but our data are concerned with more central collisions.

At impact parameters lower than 5 fm, calculations predict fusion of projectile and target with J values as high as 90 $\hbar$. However preequilibrium emission occurs during the first 100 fm/c time interval, during which 5 neutrons and 4 protons are emitted. This number of preequilibrium nucleons is in agreement with estimate based on measurement. The composite system formed at a time larger than 100 fm/c has mass A = 129, charge Z = 57, and an excitation energy of 480 MeV. Its velocity which has been reduced by preequilibrium emission reaches 1.8 cm/ns at time t = 100 fm/c. These results support the physical picture adopted here for the quantitative treatment of the azimuthal correlations. The lifetimes of 150 to 200 fm/c deduced from those correlations stand well at the beginning of the statistical stage of the obtained composite system. In addition the angular momenta so obtained from experiment and calculation have been compared in Fig. 10. The results are in agreement with an incomplete fusion process observed at impact parameters smaller than 5 fm.

5. CONCLUSION

Light charged particles, IMF and heavy residues have been measured with the 4π AMPHORA multidetector using the SARA facility in Grenoble. The origin of complex fragments has been investigated in central collisions for the ^{32}S + ^{nat}Ag system at 37.5 A·MeV incident energy. Total charge multiplicity and polar angle emission have been used to select those collisions. Azimuthal angular correlations of He - Li, Li - Li, B - B, and C - C pairs exhibit the characteristics of emission from a thermalized rotating source with an increasing preequilibrium contribution appearing at more forward angles. The evolution of lifetimes with the size of the fragments would need more investigations with a better backward identification and good statistics. Nevertheless we are able to confirm that angular momenta and lifetimes extracted from backward angle analysis agree satisfactorily with the characteristics of the emitter given by BNV computations. This microscopic approach corroborates the persistence of an incomplete fusion process responsible for statistical emission of fragments at backward angles.

References

[1] Gross, D.H.E.: Rep. Progr. Phys. **53**, 605 (1990)

[2] Moretto, L.G., Wozniak, G.J.: Ann. Rev. Nucl. Part. Sci. **43**, 379 (1993) (and references therein)

[3] Sobotka, L.G., et al.: Phys. Rev. Lett. **51**, 2187 (1983)

[4] McMahan, M.A., Moretto, L.G., Padgett, M.L., Wozniak, G.J., Sobotka, L.G., Mustafa, M.G.: Phys. Rev. Lett. **54**, 1995 (1985)

[5] Moretto, L.G., Wozniak, G.J.: Progr. Part. Nucl. Phys. **21**, 401 (1988)

[6] Pelte, D., Winkler, U., Gnirs, M., Gobbi, A., Hildenbrand, K.D., Novotny, R.: Phys. Rev. **C39**, 553 (1989)

[7] Glässel, P., Harrach, D.V., Specht, H.J., Grodzins, L.: Z. Phys. **A310**, 189 (1983)

[8] Pelte, D., Winkler, U., Bühler, M., Weissmann, B., Gobbi, A., Hildenbrand, K.D., Stelzer, H., Novotny, R.: Phys. Rev. **C34**, 1673 (1989)

[9] Grabez, B.: Phys. Rev. **C45**, R5 (1992)

[10] Bizard, G., et al.: Phys. Lett. **B302**, 162 (1993).

[11] Lopez, J.A., Randrup, J.: Nucl. Phys. **A491**, 1673 (1989)

[12] Gawlikowicz, W., Grotowski, K.: Nucl. Phys. **A551**, 73 (1993)

[13] Trockel, R., et al.: Phys. Rev. Lett. **59**, 2844 (1987)

[14] Louvel, M., et al.: Phys. Lett. **B320**, 221 (1994)

[15] Gross, D.H.E., Klotz-Engmann, G., Oeschler, H.: Phys. Lett. **B224**, 29 (1989)

[16] Pochodzalla, J., Trautmann, W., Lynen, U.: Phys. Lett. **B232**, 41 (1989)

[17] Wada, R., et al.: Phys. Rev. **C39**, 497 (1989)

[18] Nebbia, G., et al.: Phys. Rev. **C45**, 317 (1992)

[19] Benchekroun, D., et al.: Proc. Int. Winter Meeting on Nuclear Physics, Bormio (1994)

[20] Benchekroun, D.: PhD Thesis, Université Claude Bernard Lyon-1, (1994)

[21] Drain, D., et al.: Nucl. Instr. & Meth. in Phys. Res., **A281**, 528 (1989)

[22] Drain, D.: First European Biennal Workshop on Nuclear Physics, Megève, France: March 1991, ed. Guinet, D., Pizzi, J.R., World Scientific Publishing Co., p. 52 (1991)

[23] Stracener, D.W., Sarantites, D.G., Sobotka, L.G., Elson, J., Hood, J.T., Majka, Z., Abenante, V., Chbihi, A.: Nucl. Instr. & Meth. in Phys. Res., A**294**, 485 (1990)

[24] Heuer, D.: Nucl. Inst. & Meth. in Phys. Res. A**324**, 569 (1993)

[25] Désesquelles, P.: PhD Thesis, Université J. Fourier, Grenoble (1991)

[26] Magda, M.T., Alexander, J. M.: Topics in Atomic and Nuclear Collisions. ed. by Remaud, B., et al., Plenum Press, New York: 1994, p. 97

[27] Magda, M.T., et al.: Phys. Rev. C**45**, 1209 (1992)

[28] Cavata, C., et al.: Phys. Rev. C**42**, 1760 (1990)

[29] Phair, L., Bowman, D.R., Gelbke, C.K., Gong, W.G., Kim, Y.D., Lisa, M.A., Lynch, W.G., Peaslee, G.F., de Souza, R.T., Tsang, M.B., Zhu, F.: Nucl. Phys. A**548**, 489 (1992)

[30] Kox, S., et al.: Phys. Rev. C**35**, 1678 (1987)

[31] Townsend, L.W., Wilson, J.W.: Phys. Rev. C**37**, 892 (1988)

[32] Birkelund, J.R., Tubbs, L.E., Huizenga, J.R., De, J.N., Sperber, D.: Phys. Rep. **56**, 107 (1979)

[33] Blann, M.: Phys. Rev. C**31**,1245 (1985)

[34] Cole, A.J., Cherkaoui-Tadili, R., Alarja, J.: Phys. Rev. C**40**, 1265 (1989)

[35] Bougault, R., Colin, J., Delaunay, F., Genoux-Loubain, A., Hajfani, A., Le Brun, C., Lecolley, J.F., Louvel, M., Steckmeyer, J.C.: Phys. Lett. B**232**, 291 (1989)

[36] Wilson, W.K., et al.: Phys. Rev. C**41**, R1881 (1990)

[37] Elmaani, A., et al.: Phys. Rev. C**43**, R2474 (1991)

[38] Ethvignot, T., et al.: Phys. Rev. C**46**, 637 (1992)

[39] Kim, Y.D., Souza, R.T., Bowman, D.R., Carlin, N., Gelbke, C.K., Gong, W.G., Lynch, W.G., Phair, L., Tsang, M.B., Zhu, F.: Phys. Rev. C**45**, 338 (1992)

[40] Shen, W.Q., et al.: Nucl. Phys. A**551**, 333 (1993)

[41] Ethvignot, T., et al.: Phys. Rev. C**48**, 618 (1993)

[42] Phair, L., et al.: Nucl. Phys. A564, 453 (1993)

[43] Buta, A., et al.: LPCC 94 - 06 (1994)

[44] Lynch, W.G., Richardson, L.W., Tsang, M.B., Ellis, R.E., Gelbke, C.K., Warner, R.E.: Phys. Lett. 108B, 274 (1982)

[45] Chitwood, C.B., et al.: Phys. Rev. C34, 858 (1986)

[46] Dossing, T.: Licentiat thesis, University of Copenhagen (1979)

[47] Ajitanand, N.N., La Rana, G., Lacey, R., Moses, D.J., Vaz, L.C., Peaslee, G.F., de Castro Rizzo, D.M., Kaplan, M., Alexander, J.M.: Phys. Rev. C34, 877 (1986)

[48] Ajitanand, N.N., et al.: to be published in Nucl. Instr. & Meth. in Phys. Res.

[49] Rivet, M.F., et al.: Proc. Int. Winter Meeting on Nucl. Phys.: Bormio, (1993)

[50] Zhu, F., et al.: Phys. Lett. B322, 43 (1994)

[51] Cerutti, C., Guinet, D., Chiodelli, S., Demeyer, A., Zaïd, K., Leray, S., Lhenoret, P., Mazur, C., Ngô, C., Ribrag, M., Lleres, A.: Nucl. Phys. A453, 175 (1986)

[52] Bauge, E., et al.: Phys. Rev. Lett. 70, 3705 (1994)

[53] Bauge, E.: PhD Thesis, Univeristé J. Fourier, Grenoble, (1994)

[54] Bonasera, A., Gulminelli, F.: Phys. Rep. 243, 1 (1994)

Figure captions

Figure 1 : $^{32}S + ^{nat}Ag$ reaction at 37.5 A· MeV : Non - triggered and triggered multiplicity distributions of IMF detected in 4π . The multiplicity distributions are gated by three intervals (ΔM) of total charged particle multiplicity, associated with peripheral, semi-central and central collisions.

Figure 2 : $^{32}S + ^{nat}Ag$ reaction at 37.5 A· MeV : (a) experimental charged particle multiplicity distribution, (b) relationship between the reduced impact parameter and the total multiplicity.

Figure 3 : Average total multiplicity versus IMF emission polar angle.

Figure 4 : Charged particle multiplicity distributions gated by at least one or two Li fragments detected at 16° - 78° polar angles (open circles and triangles). The primary distribution (black circles) was obtained from selected events having at least one IMF in the whole AMPHORA.

Figure 5 : λ_1 and λ_2 values versus the reduced impact parameter extracted from measurements.

Figure 6 : Mass distribution (shown in the inset) and velocity spectrum of heavy residue - like fragments (histogram) at $\theta_{lab}=8°$. Full and open circles denote the spectrum gated by charged particle multiplicity $\Delta M2$ and $\Delta M3$ respectively.

Figure 7 : Measured azimuthal angle correlations of He - Li pairs. Simulations with MODGAN code involving an emission time of 50 10^{-22}s are displayed by solid lines.
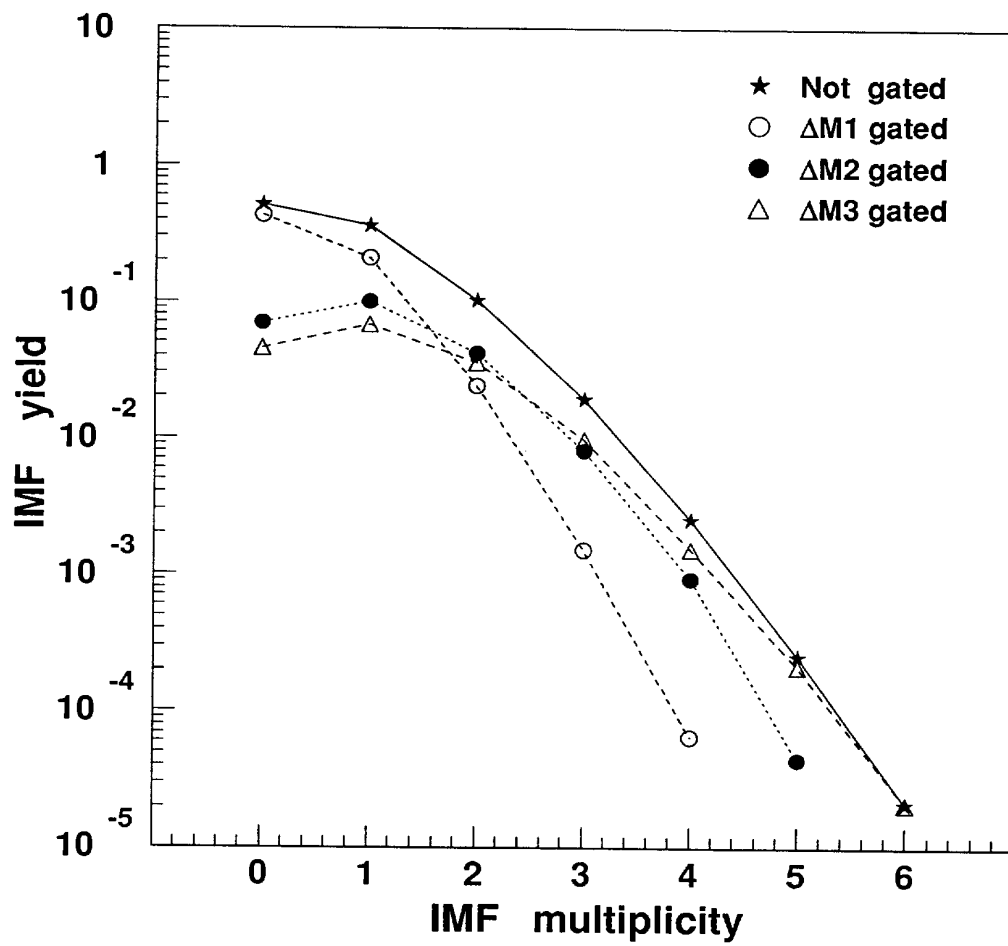
Figure 8 : Measured (full circles) azimuthal angle correlations (not gated) of Li - Li, B - B, and C - C pairs detected at 20° and 31°. Simulations with MODGAN code for J = 100 $\hbar$ and various time delays are displayed by solid and dashed lines.
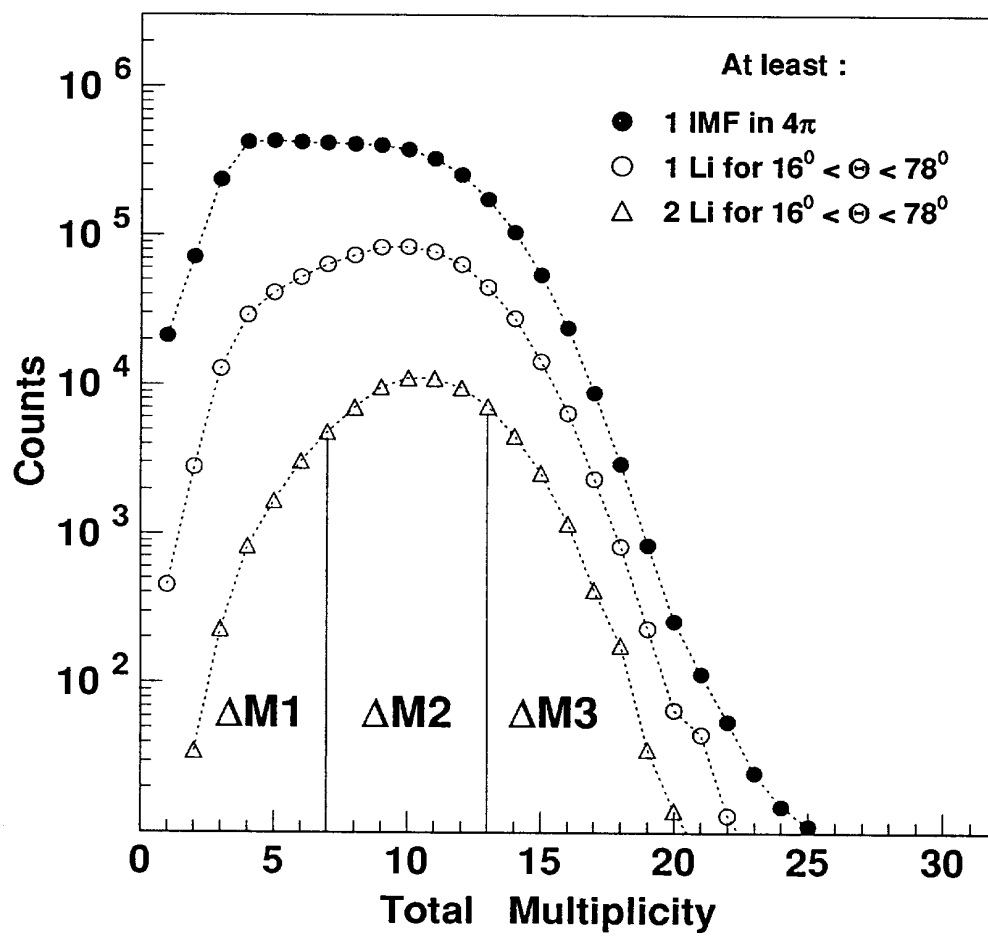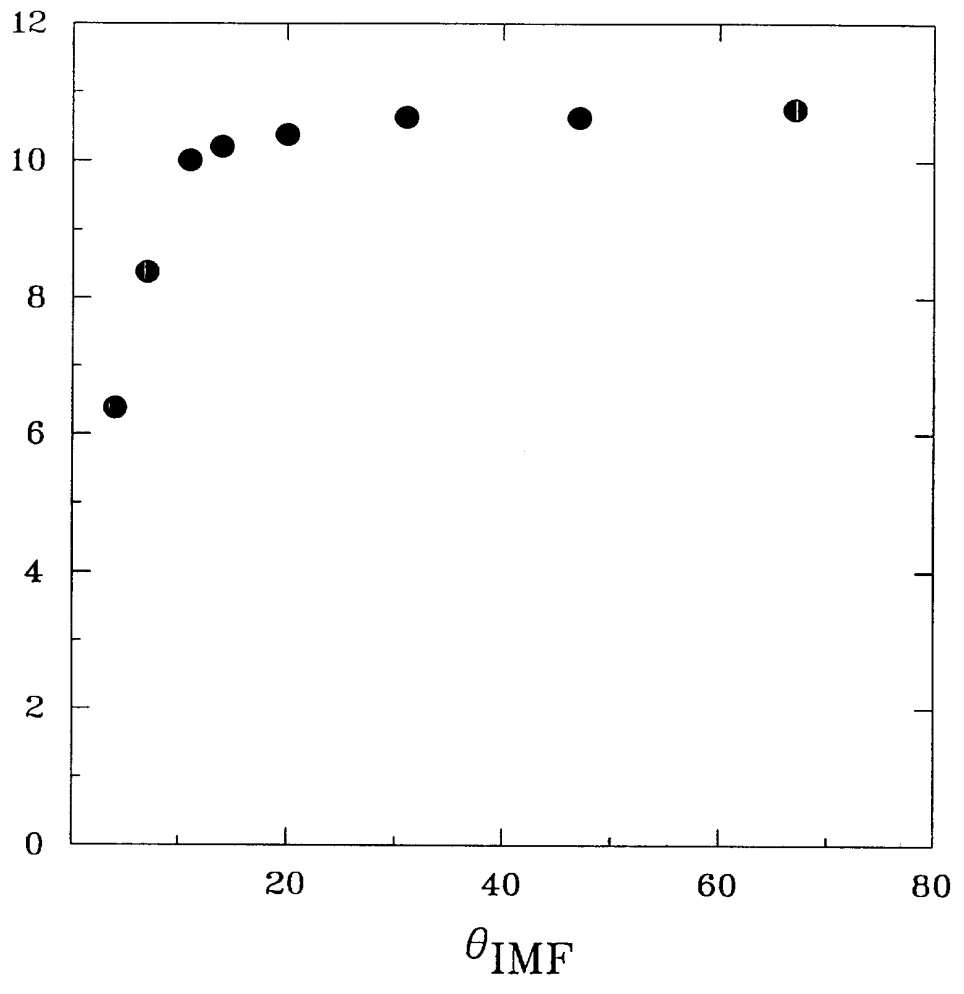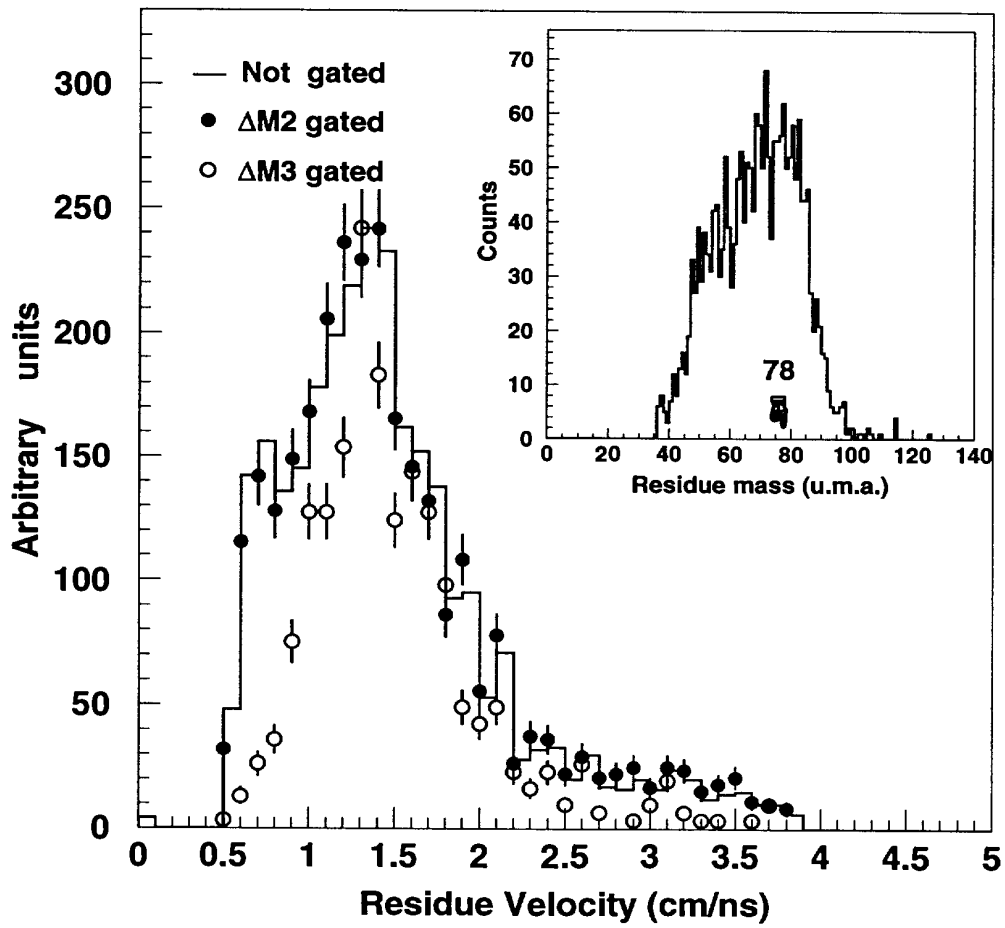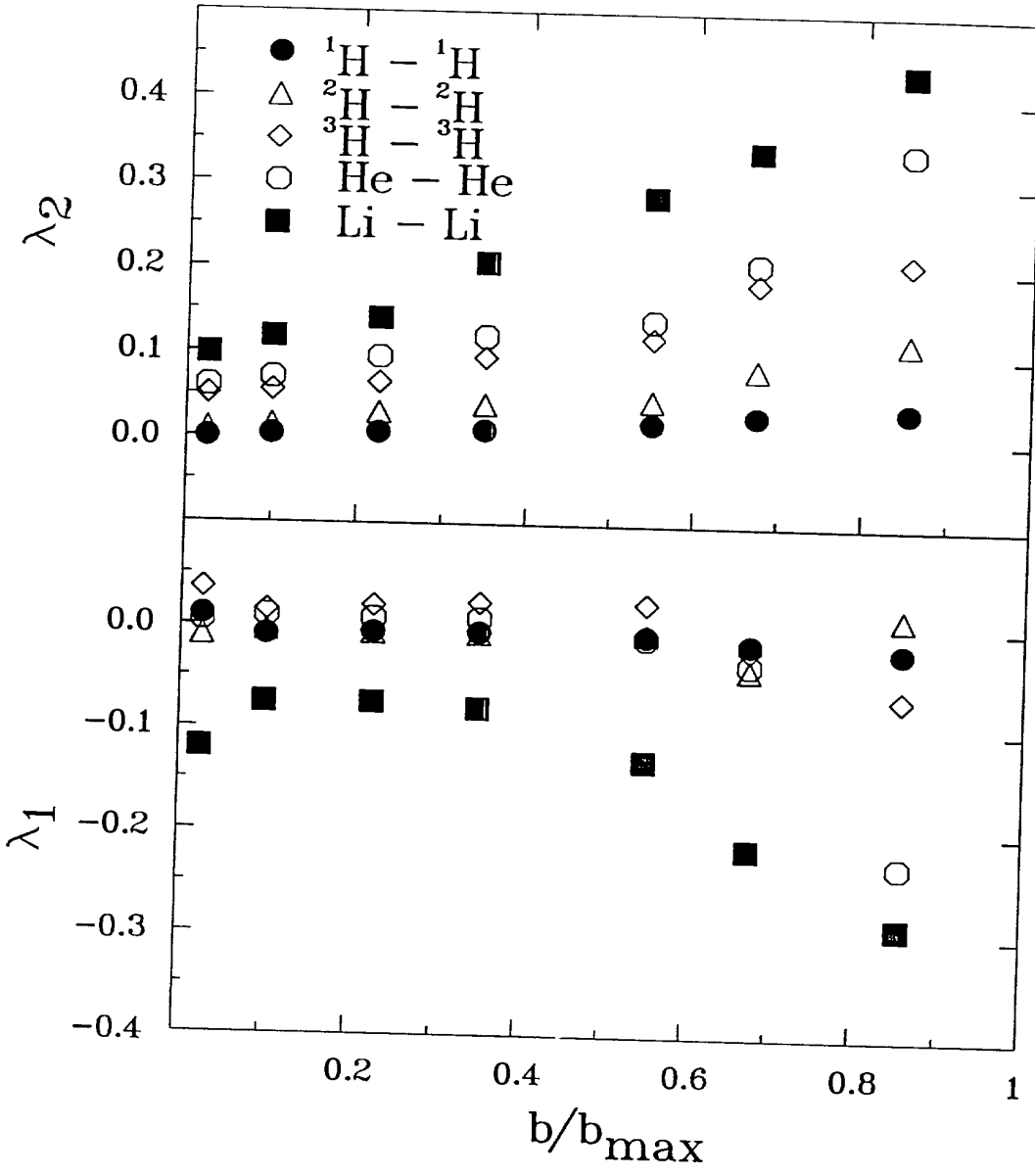
Figure 9 : Measured (full circles) azimuthal angle correlations (not gated) of Li - Li pairs detected at 31° and 47°. Simulations with MODGAN code for J = 80 $\hbar$ and various time delays are displayed by solid and dashed lines. The best fit is obtained for a time delay equal to 7 10^{-22}s (solid line).

Figure 10 : Angular momenta predicted by BNV calculations for the system $^{32}S +^{nat} Ag$ at 37.5 A·MeV compared to experimental data. BNV simulations are represented by histogram.
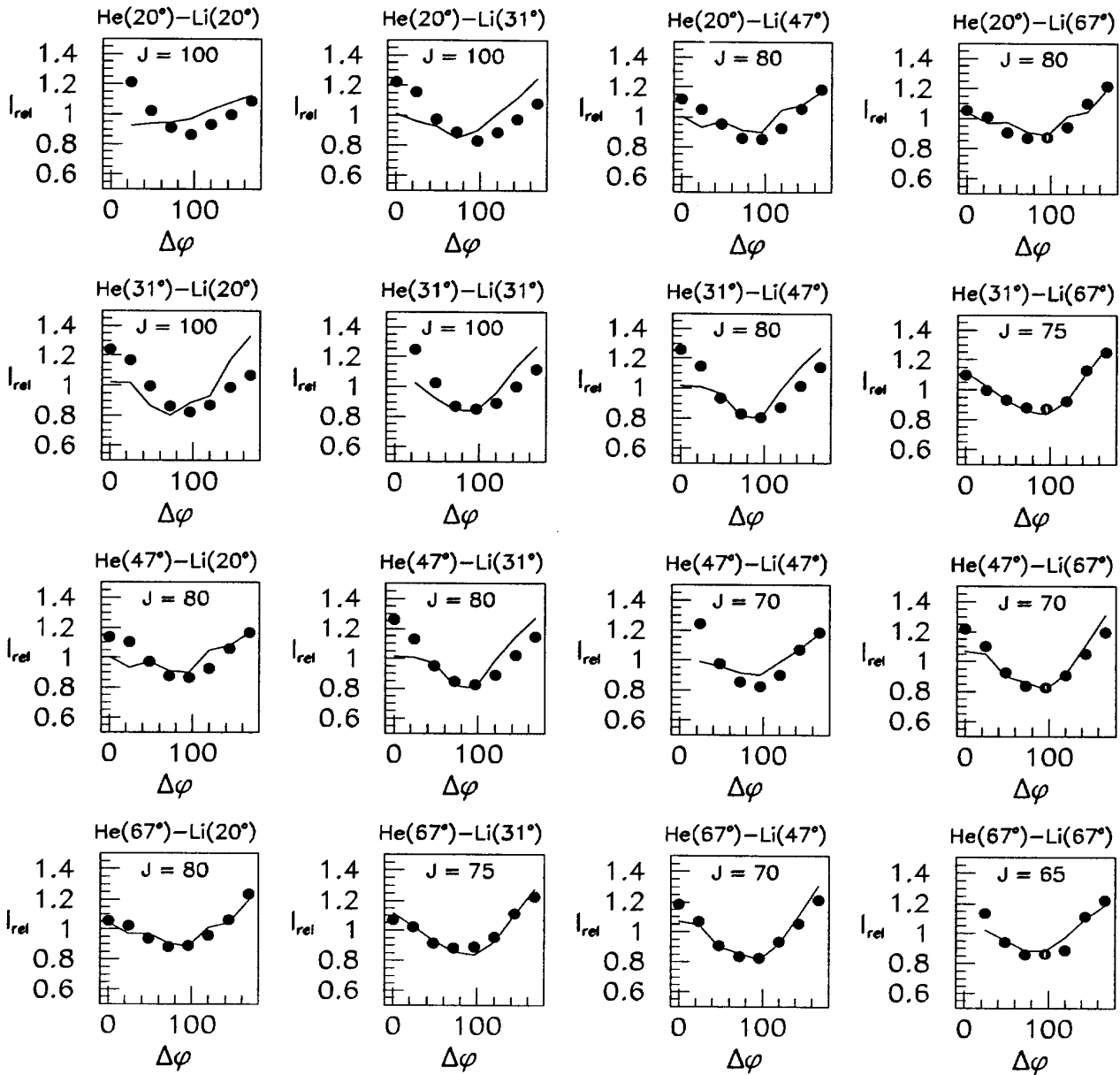
Li(20°)-Li(31°)

$$I_{rel.}$$

- - - $\tau = 5$
- · - · $\tau = 20$
——— $\tau = 50$

$\Delta\varphi$

B(20°)-B(31°)

$$I_{rel.}$$

- · - · $\tau = 2$
——— $\tau = 5$

$\Delta\varphi$

C(20°)-C(31°)

$$I_{rel.}$$

——— $\tau = 1$
- · - · $\tau = 2$

$\Delta\varphi$

Li(31$^{\mathrm{o}}$) - Li(47$^{\mathrm{o}}$)